Tuning of the Dispersion of Ligand-Free ZnO Quantum Dots in Polymer Matrices with Exfoliated Nanoplatelets

Dazhi Sun,[§,†] W. Neil Everett,[†,‡] Minhao Wong,[§] Hung-Jue Sue,*[,†] and Nobuo Miyatake[||]

Polymer Technology Center, Department of Mechanical Engineering, Texas A&M University, College Station, Texas 77843-3123; Exoteric Instruments, LLC, 604 Basie Bnd, Austin, Texas 78613; Frontier Materials Development Laboratories, Kaneka Corporation, 5-1-1 Torikai-Nishi, Osaka, Settsu 566-0072, Japan; and Kaneka Texas Corporation, 6161 Underwood Rd, Pasadena, Texas 77507

Received August 31, 2008; Revised Manuscript Received January 2, 2009

ABSTRACT: This paper concerns the experimental observation of dispersion tuning ligand-free ZnO quantum dots down to the single-particle level, in polymer matrices, through the use of exfoliated ZrP nanoplatelets. High-resolution transmission electron microscopy and optical transmission spectroscopy reveal that the degree of dispersion depends strongly on the relative volume fractions of each nanoscale constituent, and polymer nanocomposites prepared with this method exhibit nearly identical optical transmittance spectra to that of their neat counterparts. Dynamic and kinetic analyses and control experiments involving the dispersion of ZnO in organic solvents using nanoplatelets suggest that the dispersion mechanism likely involves nanoplatelets locally and transiently altering the thermodynamic character of the matrix, perhaps through polarization. Hence, quantum dots achieve their dispersed state through more favorable interactions with the surrounding medium brought about by the presence of nearby diffusing nanoplatelets. This work demonstrates the ability to stabilize nanoscale particles without the use of covalent functionalization or physisorbed macromolecules and at a low dispersant volume fraction. Furthermore, the broad applicability of these results could extend into many areas of nanocomposites research.

Introduction

Semiconductor nanocrystals, also known as quantum dots (QDs), possess outstanding optoelectronic properties that are of practical use in many electronic, photonic, and biological applications.[1−3] These exceptionally useful characteristics arise from both quantum size effects and their enormous surface-to-volume ratio.[4] By varying QD diameter, the degree of quantum confinement is tuned, which defines their optoelectronic response; the large fraction of noncoordinated surface atoms dictates many of their thermodynamic properties. Yet, these two characteristics are linked intimately with the degree to which the QDs are dispersed within a medium or supporting matrix.

As individual quantum dots increase in size, optical absorption and emission undergo a red shift, which is generally observed in highly dispersed colloids.[5,6] Likewise, in systems where colloidal aggregates are formed, QDs exhibit red-shifting as aggregate size increases.[7] It has been demonstrated that electronic energy transfer can occur between neighboring QDs through long-range coupling at interparticle separations of up to 10 nm,[8,9] and QDs begin to display bulk material properties when they come into direct contact and reach a critical aggregate size.[10] Moreover, similar phenomena have been observed in ligand-free QD powder[11] and highly aggregated ligand-free QDs in polymer matrices.[12] As a result, tuning the degree of QD dispersion in composites is a requisite for achieving specific material attributes.

Surface area-to-volume ratio drops abruptly as the degree of QD aggregation increases, and this reduces their usefulness in many ways. For example, QD aggregation in polymers may affect adversely the efficiency of photovoltaic devices, such as solar cells, by reducing the interfacial area and thus decreasing power-conversion efficiency.[13,14] Physical properties of polymer matrices, e.g. thermal stability, modulus, toughness, etc., may be significantly compromised by a reduction in the interfacial surface area resulting from QD aggregation.[15] Additionally, highly aggregated particulate matter within transparent matrices inevitably causes substantial light scattering that restricts the use of polymer nanocomposites to a limited set of optical applications.[16,17]

Within the colloidal regime, QDs are generally stabilized through surface modification using covalently bound ligands or adsorbed macromolecules.[5,18−20] Solution mixing is another straightforward approach to achieve better dispersion of inorganic nanofillers in polymers, but it requires the particles to be stable in a dispersing solvent that is also miscible with the polymer matrix.[21] In many cases, though, phase separation between the polymer and nanofiller occurs after solvent extraction even if these preliminary criteria are satisfied.[22]

This report introduces a new approach to disperse ligand-free colloidal zinc oxide (ZnO) QDs in polymer matrices through the addition of exfoliated α-zirconium phosphate (ZrP) nanoplatelets (NPs). Here, high-resolution transmission electron microscopy (HRTEM) reveals that the dispersion state of the QDs in the polymer matrix can be tuned from micron-sized aggregates down to individual QDs by adjusting NP concentration. The polymer hybrid ZnO/ZrP nanocomposites that contain well-dispersed QDs also exhibit nearly identical optical transmittance spectra to that of our neat epoxy samples. Additionally we found that, although QDs readily form aggregates when added to acetone and methanol, the presence of NPs at a sufficient volume fraction leads to QD dispersion down to nanoscale clusters and likely individual dots within the solvent. We first hypothesized that the addition of nanoplatelets to a polymer melt or uncured epoxy could act to disrupt aggregation of nanoparticles such as QDs, which would improve their dispersion within the composite. On the basis of our experimental results and dynamic and kinetic analyses, however, we propose that the dispersion mechanism most likely involves ZrP

* To whom correspondence should be addressed: e-mail hjsue@tamu.edu; ph 979.845.5024; fax 979.845.3081.
[†] Texas A&M University.
[‡] Exoteric Instruments, LLC.
[§] Kaneka Corporation.
[||] Kaneka Texas Corporation.

10.1021/ma801979c CCC: $40.75
Published on Web 02/10/2009

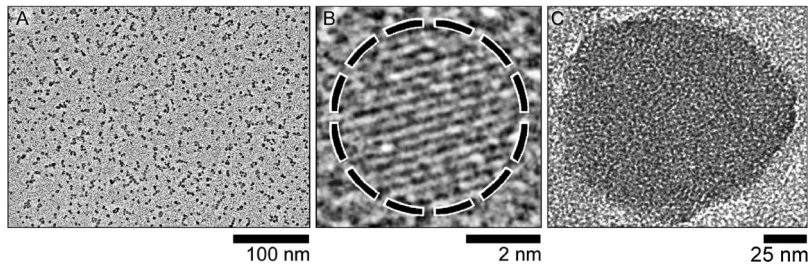

Figure 1. (A) Low- and (B) high-magnification HRTEM images of ligand-free colloidal ZnO QDs. Dashed line in (b) demarks the perimeter of the QD. (C) HRTEM of a single ~100 nm ZrP NP exfoliated with TBA^+OH^-, representative of the typical geometry.

NPs thermodynamically altering local matrix interactions with the QDs. Extensions of the approach described in this report may be ideal for a variety of applications including, but not limited to, photovoltaic devices, thermal and optical stabilizers, and antimicrobial coatings, wherein QD functionalization often negatively impacts material performance.

Experimental Section

Nanoplatelet and Quantum Dot Preparation. Colloidal ZnO QDs were synthesized by hydrolyzing 99% zinc acetate dihydrate (Fluke) in a basic methanol solution in the absence of surfactants and ligands. QDs were then purified through an aggregation/redispersion procedure similar to one outlined in a previous report, which led to individually dispersed ZnO QDs and a dispersion with 99.8% of its ion impurities removed after only three purification cycles.[23] Purified QDs were then redispersed in methanol to a final concentration of 32 mg mL^{-1}, and their size was characterized with a JEOL 2010 HRTEM operated at 200 kV, as shown in Figure 1A,B. Our ZnO QDs were highly crystalline and had a narrow size distribution with an average diameter of 5.0 ± 0.3 nm.

ZrP NPs having average dimensions of $\sim 100 \times 0.7$ nm were used in this study and synthesized according to methods detailed in our previously reported work.[24] Following synthesis, the pristine, stacked ZrP NPs were exfoliated into single platelets in an aqueous solution through the use of tetra-*n*-butylammonium hydroxide (TBA^+OH^-, 1.0 M solution in methanol, Sigma-Aldrich) at a molar ratio of $ZrP:TBA^+OH^- = 1.25$. X-ray diffraction data have been used to verify the efficacy of this method by demonstrating the existence of fully exfoliated platelets.[25] The single exfoliated ZrP NP shown in the TEM image in Figure 1C is representative of the typical NP shape.

It should be mentioned that ZrP NPs possess several attractive attributes that make them model nanostructures for composites research. NPs have been utilized as fillers to produce materials that exhibit better barrier properties, enhanced flame retardancy, improved mechanical toughness, etc.[26−28] Specifically, ZrP is a synthetic material with a well-known chemical structure and a high degree of purity,[29] and full exfoliation of ZrP NPs can be achieved in aqueous solutions.[30] By using centrifugation and redispersion, NPs can be transferred into organic solvents such as acetone and methanol, and that dispersion can then be incorporated into epoxy resins and many other polymers without the NPs aggregating and losing their exfoliated state.[25] Finally, ZrP NP diameter can be tuned from dozens of nanometers up to microns,[24] which allows us to understand the impact aspect ratio has, if any, on their ability to disperse nanoscale constituents such as QDs.

Epoxy Nanocomposite Preparation. To create our epoxy nanocomposites, diglycidyl ether of bisphenol A (DGEBA) epoxy resin (DER 332 epoxy resin, Dow Chemical Co.) with an average epoxide equivalent weight of 174 was first dissolved in acetone containing exfoliated and dispersed ZrP NPs, and then a dispersion of purified ZnO QDs in methanol was added to the mixture. The solvents were then volatilized in a roto-vapor under vacuum at 80 °C for 1 h. Following solvent evaporation, the epoxy mixture was clear and appeared to be free of QD aggregates; epoxy mixtures prepared without NPs were cloudy following this step. After being degassed at 100 °C for 1 h, a stoichiometric amount of the curing agent 4,4′-diaminodiphenyl sulfone (DDS, Sigma-Aldrich) was added to the epoxy. This mixture was heated rapidly to 130 °C and held at that temperature until the DDS was fully dissolved. The mixed epoxy was then poured into a preheated glass mold coated with mold-release agent (Frekote44-NC, Henkel), cured in an oven at 180 °C for 2 h, postcured at 220 °C for another 2 h, and then slowly cooled to room temperature. Samples containing both ZnO QDs and ZrP NPs are hereafter designated as either "epoxy/ZnO/ZrP" or "epoxy hybrid nanocomposites".

Epoxy hybrid nanocomposites with different volume fractions (ϕ_{ZnO} and ϕ_{ZrP}) of ZnO QDs and ZrP NPs were prepared for this study. For comparison purposes, neat epoxy samples without fillers and epoxy composites containing only ZnO QDs ("epoxy/ZnO") were also prepared by the same curing protocol described above. All epoxy composites were characterized with HRTEM and the microscopy samples were produced through ultramicrotomy (Reichert-Jung Ultracut-E microtome) to create thin sections of around 80 nm in thickness. Ten samples were prepared for each nanofiller combination, and data and HRTEM images presented here are representative of results from each composite group.

Results and Discussion

Varying Nanofiller Volume Fractions. HRTEM images of an epoxy/ZnO cross section and various epoxy hybrid nanocomposites containing different QD and NP volume fractions are given in Figure 2. Generally speaking, ligand-free colloidal ZnO QDs are unstable in epoxy resins;[23] thus, large (hundreds of nanometers to microns) ZnO aggregates form after their incorporation into the non-cross-linked polymer, as shown in Figure 2A. After adding exfoliated ZrP NPs, however, nanoscale dispersion of ZnO QDs is achieved. At $\phi_{ZnO} = 0.004$ and $\phi_{ZrP} = 0.002$, QDs are well dispersed with the average 2D aggregate containing around 5−10 QDs (Figure 2B and inset). If the QD concentration increases to $\phi_{ZnO} = 0.008$ and the NP loading is maintained at $\phi_{ZrP} = 0.002$, QDs are still homogeneously dispersed, but the average aggregate contains 10−20 particles (Figure 2C). On the other hand, if the nanocomposite is composed of either ZnO at $\phi_{ZnO} = 0.002$ and ZrP NPs at $\phi_{ZrP} = 0.002$ (Figure 2D) or ZnO at $\phi_{ZnO} = 0.004$ and ZrP at $\phi_{ZrP} = 0.004$ (Figure 2E), the QDs reach a completely dispersed state, more or less. Insufficient NP loading, e.g., $\phi_{ZnO} = 0.004$ with $\phi_{ZrP} = 0.0004$ (Figure 2F), led to large aggregate formation, similar to that observed in the epoxy/ZnO composite cross section shown in Figure 2A.

To describe ZnO aggregate size in more quantitative terms, analysis of HRTEM images using ImageJ (freeware from the National Institutes of Health) yielded two-dimensional radius of gyration (R_g^{2D}) estimates, which will be used later in this paper to help explain the nature of the dispersion mechanism. Figure 3 shows the R_g^{2D} distributions found for each composite system. The maximum projected length of a diffusion-limited aggregate, L, from a 2D TEM image is related to the three-dimensional radius of gyration (R_g^{3D}) of the aggregate through $L/3 \cong R_g^{3D}$, with $R_g^{3D} = 1.24R_g^{2D}$.[31,32] Note that these approximations begin to break down for aggregates smaller than

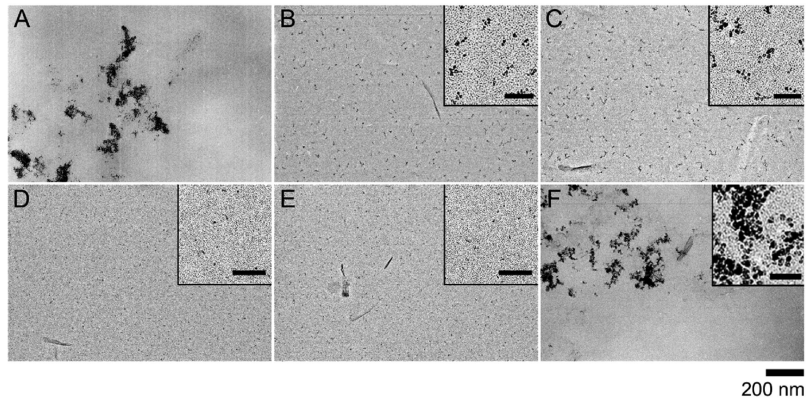

Figure 2. HRTEM images of epoxy nanocomposites containing (A) $\phi_{ZnO} = 0.004$, (B) $\phi_{ZnO} = 0.004$ + exfoliated ZrP at $\phi_{ZrP} = 0.002$, (C) $\phi_{ZnO} = 0.008$ + exfoliated ZrP at $\phi_{ZrP} = 0.002$, (D) $\phi_{ZnO} = 0.002$ + exfoliated ZrP at $\phi_{ZrP} = 0.002$, (E) $\phi_{ZnO} = 0.004$ + exfoliated ZrP at $\phi_{ZrP} = 0.004$, and (F) $\phi_{ZnO} = 0.004$ + exfoliated ZrP at $\phi_{ZrP} = 0.0004$. Insets are from the same composite at a higher magnification with scale bars of 50 nm (B, C, D, E) and 25 nm (F).

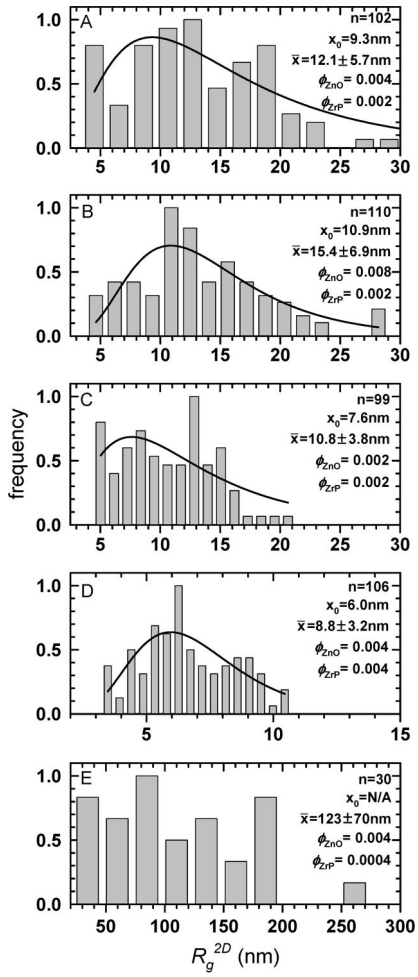

Figure 3. Distributions of R_g^{2D} found from analysis of TEM images, where n is the number of aggregates used to create each distribution. Log-normal fits are given for (A−D) to yield the value of the distribution's peak (x_0), and the arithmetic mean ($\bar{x}$) of the distribution is also given.

about five particles, so the estimates in Figure 3 involving clusters of this size and smaller are not very meaningful. Nevertheless, this method is valid for defining the dimensions of the larger aggregates seen in our experimental systems.

Optical Transmittance Spectra. UV−vis spectra (Figure 4A) of neat epoxy and epoxy nanocomposites were collected on a Hitachi UV−vis−NIR spectrophotometer (model U-4100). Samples were cut and then polished simultaneously using 1200, 2400, and then 4000 grit paper, and the final refinement was completed with 1 μm diamond paste to achieve sufficient surface smoothness for optical transmittance measurements. The final thickness of each sample group was around 2 mm with a standard deviation in thickness within each group of ~0.05 mm. Figure 4A shows the light transmission spectra of neat epoxy, epoxy/ZnO, and epoxy/ZnO/ZrP specimens. The neat epoxy sample filtered wavelengths below ~370 nm and reached a maximum transmittance of about 91% within the range examined. The light transmittance T_m of a pure epoxy matrix for a monochromatic source is estimated by the following equation: $T_m = (1 - R)^2 \exp(-\alpha h)$, where R is the surface reflection and is defined by $R = (n - 1)^2/(n + 1)^2$, α is the loss factor, h is the thickness of the specimen, and n is the refractive index of the neat epoxy matrix.[33] The refractive index of a typical DGEBA/amine system varies from 1.54 to 1.58 due to density variations.[34] Assuming $\alpha = 0$ and $n = 1.56$, the estimated maximum light transmittance of the neat epoxy should be about 90.5%, which is very close to our experimental finding of 91%. Therefore, α of our neat epoxy system approaches 0 for $\lambda >$ 600 nm.

All of the epoxy/ZnO/ZrP nanocomposites containing well-dispersed ZnO QDs and exfoliated ZrP NPs have transmittance spectra very similar to that of the neat epoxy system, except between 370 and 550 nm where epoxy/ZnO/ZrP specimens show a slightly red-shifted and attenuated transmittance. This is most likely due to the ZnO QDs absorbing light within this range. In sharp contrast, epoxy/ZnO nanocomposites containing large ZnO aggregates (see Figure 2A) exhibit a much lower transmittance than both the neat epoxy and hybrid nanocomposites, leveling off at ~55% near 600 nm and above. Photographic images of the neat epoxy, epoxy/ZnO, and an epoxy/ZnO/ZrP nanocomposite are shown in Figure 4B. The specimen containing only ZnO QDs is translucent (Figure 4B(ii)), while the epoxy hybrid nanocomposite filled with aggregates composed, on average, of about 10 QDs (Figure 4B(iii)) is highly transparent and similar to the neat epoxy (Figure 4B(i)). Qualitatively, the light transmission spectra and photographic images clearly demonstrate that the hybrid nanocomposites contain ZnO QDs with a much better degree of dispersion than that seen in the epoxy/ZnO system, which is in agreement with our HRTEM results.

As for the case of the epoxy hybrid nanocomposites where QDs are not well dispersed (Figure 2F), optical transmittance is still greater than that of the epoxy/ZnO nanocomposite, clearly indicating that exfoliated NPs impact the degree of QD dispersion, even at very low volume fractions. On the basis of

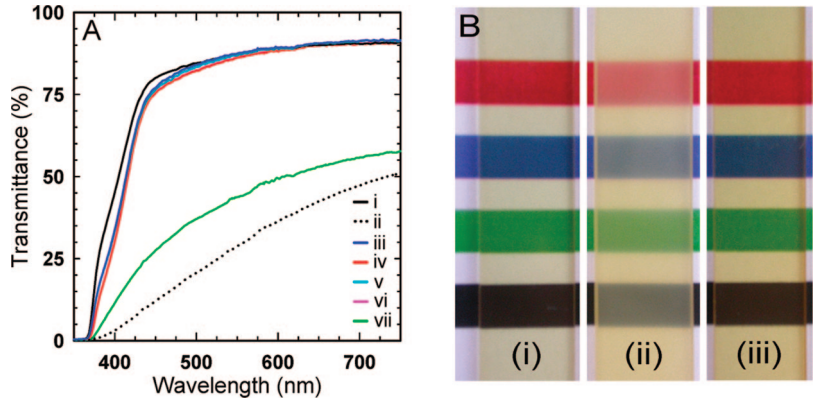

Figure 4. (A) Light transmission spectra of (i) neat epoxy, (ii) epoxy/ZnO ($\phi_{ZnO} = 0.004$), (iii) $\phi_{ZnO} = 0.004$ + exfoliated ZrP at $\phi_{ZrP} = 0.002$, (iv) $\phi_{ZnO} = 0.008$ + exfoliated ZrP $\phi_{ZrP} = 0.002$, (v) $\phi_{ZnO} = 0.002$ + exfoliated ZrP at $\phi_{ZrP} = 0.002$, (vi) $\phi_{ZnO} = 0.004$ + exfoliated ZrP at $\phi_{ZrP} = 0.004$, and (vii) $\phi_{ZnO} = 0.004$ + exfoliated ZrP at $\phi_{ZrP} = 0.0004$ and (B) photographic images of samples (i), (ii), and (iii).

the spectral data, if QDs are dispersed down to nanoscale aggregates containing fewer than 20 particles, light scattering and absorption within the range of wavelengths examined are minimal. As such, the transparency of the polymer matrices can be maintained, which is highly desirable for many composites applications.

Quantum Dot Dispersion Mechanism. NP-assisted dispersion of ZnO QDs could involve a single or several chemical or physical mechanisms. For example, diffusing NPs could alter the kinetics of aggregate formation by physically disrupting the association of QDs (note that hydrodynamic mixing is not relevant here due to the tremendously low Reynolds number at these length scales (10^{-9}−10^{-7} m) and diffusive rates ($\sim 10^{-8}$ m/s)). In an alternative fashion, the ligand-free ZnO QDs could be incidentally passivated by an adsorbed layer of excess TBA that remains after the NP exfoliation step. Furthermore, ZrP NPs and/or excess TBA could be shifting the pH or interacting with the matrix to sequester ZnO-phobic portions of the polymer. Various control experiments were conducted, therefore, to determine the extent to which any one of these factors plays a role in ZrP dispersing ZnO QDs at such low NP volume fractions.

The most obvious control experiment to perform was to determine if excess TBA was behaving as a surfactant and absorbing to the ZnO surface, thereby forming an electrosteric stabilizing layer that would facilitate QD dispersion. We prepared epoxy/ZnO samples with TBA^+OH^- but without NPs. More specifically, the samples contained ZnO at $\phi_{ZnO} = 0.004$ and TBA at a loading equal to that of the TBA mass used within the sample composed of exfoliated ZrP at $\phi_{ZrP} = 0.002$ (see cross section shown in Figure 2B). Just as in the case of epoxy/ZnO, we observed large ZnO aggregates in HRTEM images, and specimens were translucent with nearly identical optical properties to that of the epoxy/ZnO cross section shown in Figure 2A and Figure 4A(ii), indicating that excess, freely diffusing TBA within the epoxy matrix is not responsible for ZnO QD stabilization.

To understand whether NPs could be breaking up or slowing down the formation of QD aggregates in a physical or dynamic manner, several experiments were conducted. Here, we directly compare the characteristic time scale of QD aggregate formation to the time scales of NP and QD diffusion to demonstrate the validity of this mechanism. We start by assuming that the QD and NP volume fractions within our systems are below the limit that results in multiparticle hydrodynamic interactions and an associated increase in effective viscosity.[35]

In order to model the diffusive behavior of our 100 nm ZrP NPs, their geometry can be approximated as oblate ellipsoids with principal dimensions of $2a$, $2b$, and $2c$ with $b = c$ and $b/a \gg 1$, where a represents NP thickness and b is equivalent to NP radius, r_{ZrP}. The friction factors take the following form:[36] $f_{||} = 16\pi\mu_0(a^2 - b^2)/[(2a^2 - b^2)S - 2a]$ and $f_\perp = 32\pi\mu_0(a^2 - b^2)/[(2a^2 - 3b^2)S + 2a]$, where μ_0 is the matrix/medium viscosity at infinite particle dilution and S is defined by $S = [2/(b^2 - a^2)^{1/2}] \tan^{-1}[(b^2 - a^2)^{1/2}/a]$. As $b/a \rightarrow \infty$, the friction factors can be simplified to $f_\perp = 32\mu_0 r_{ZrP}/3$ and $f_{||} = 16\mu_0 r_{ZrP}$. The perpendicular and parallel diffusion coefficients of the NPs are then given by $D_\perp = kT/f_\perp$ and $D_{||} = kT/f_{||}$, and the effective diffusive coefficient of the ZrP NPs, $\bar{D}_{ZrP}$, is described as[37] $\bar{D}_{ZrP} = (D_{||} + 2D_\perp)/3$.

We approximate the diffusion coefficient of a spherical ZnO QD of radius r_{ZnO} with the Stokes−Einstein equation given by[38]

$$D_{ZnO} = \frac{kT}{6\pi\mu_0 r_{ZnO}} \quad (1)$$

The ratio of the diffusion coefficients of QDs to NPs is then

$$\frac{D_{ZnO}}{\bar{D}_{ZrP}} = \frac{2}{\pi}\left(\frac{r_{ZrP}}{r_{ZnO}}\right) \quad (2)$$

From eq 2, the diffusion coefficient of a 5 nm ZnO QDs is about 12.5 times greater than that of 100 nm ZrP NPs if the two species are freely diffusing. Once cross-linking is initiated, on the other hand, this ratio becomes invalid because NP mobility is far more affected by local polymer entanglements than that of QDs because of their geometry and size. As the matrix becomes more cross-linked, the diffusive rates of both colloidal species will drop significantly and eventually tend to zero. Because of the difference in diffusive rates, we can safely assume that NPs would be unable to substantially affect the formation of ZnO QD aggregates through purely kinetic means, especially if the clusters are formed on short time scales through diffusion-limited aggregation. Although we do not know the reaction rate of QD association, we observed the formation of QD aggregates within the epoxy resin when NPs are absent only moments after the addition of ZnO, so we can reasonably approximate the clustering as diffusion-limited. Further refuting the argument that QD clustering is physically disrupted by diffusing NPs is the fact that an undisturbed and non-cross-linked epoxy resin mixture that we prepared with ZnO QDs at $\phi_{ZnO} = 0.004$ and exfoliated ZrP at $\phi_{ZrP} = 0.004$ has now remained devoid of visible QD clusters for over one year. Finally and most importantly, the observation of individually dispersed QDs and small clusters in our epoxy composites (Figure 2D,E) cannot be explained by NP disruption of aggregate formation.

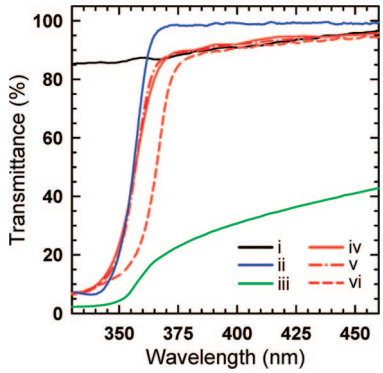

Figure 5. Optical transmittance spectra of (i) 100 nm exfoliated ZrP NPs dispersed in acetone, (ii) ZnO QDs dispersed in methanol, (iii) ZnO QDs in acetone, (iv) ZnO QDs + ZrP NPs in acetone at 0 h, (v) ZnO QDs + ZrP NPs after 3 h, and (vi) ZnO QDs + ZrP NPs after 1 year. ZnO and ZrP are at concentrations of 3 mg/mL for all cases.

Also of importance in this discussion is to note that experimental results in the literature indicate that the diffusion coefficient of nanoparticles of this size, freely moving in polymer melts, can be up to 200 times greater than that predicted by eq 1,[39] while NP diffusion at infinite dilution is accurately predicted by the above analysis.[40] It has been shown with molecular dynamics simulations that the Stokes−Einstein equation is valid for nanometer-scale particles larger than the radius of gyration of the suspending polymer.[41] Because the contour length of DER 332 is ∼2 nm,[42] the QDs used in this study are several times larger than the monomer's radius of gyration, so we can safely assume eq 2 is reasonable. Furthermore, any deviation from this model says that our QDs would be diffusing at faster rates than we have predicted, which bolsters our argument that the NPs cannot be disrupting aggregate formation through solely kinetic means.

When directly added to hexane, acetone, methanol, and deionized water, ZnO QDs aggregate and drop out of suspension. The observed rates of ZnO aggregate formation and sedimentation are quite different in these media and have the following ranking in order from slowest to fastest: methanol, acetone, DI water, and then hexane. Of interest is the fact that this order also follows the ranking of dipole moment magnitudes of these solvents, with methanol having the largest of the four. In the case of acetone and methanol, we observed that the addition of ZrP NPs prior to the addition of QDs prevents visible QD aggregates from ever forming, and NPs added after QD aggregates are allowed to form, result in the breakup of large clusters into much smaller aggregates. In contrast, ZrP NPs are ineffective at preventing QD aggregates from forming if the dispersion is produced in water or hexane. Optical transmittance spectra of dispersion experiments in acetone are given in Figure 5. The optical transmittance spectrum of ZnO QDs (3 mg mL^{-1}) in acetone without the addition of NPs shows a significant attenuation (Figure 5(iii), whereas the addition of ZrP NPs at 3 mg mL^{-1} prevents or significantly reduces the formation of aggregates. After one year, the stability of this same suspension remains nearly unchanged (Figure 5(vi)) with only a small increase in average aggregate size, evidenced by the red-shifted spectrum.

These experimental results with simple solvents are important because they show that the NPs are impacting the medium-QD interactions, but how NPs bring about this change is not obvious. One possible explanation is that NPs could be polarizing the medium in the vicinity of a QD. In the case of methanol and acetone, electrons on the oxygen atom are relatively mobile, and these solvents have the potential to become more electronegative in the presence of a NP through dipole−dipole interactions, which would increase the interaction of the solvent with the Zn atoms on the surface of the QD. In the case of water and hexane, the dipole moments may be below the polarization threshold that enhances the polar bonding between the solvent and QDs to the point where the QDs redisperse. For the epoxy used in our study, the monomer has two ethers on opposite ends of the molecule, which also have the potential to become highly polarized. Moreover, we have achieved successful dispersion in other polymers with ether groups (e.g., DER 331 epoxy and PMMA; results not shown here), indicating polarizability may be the key characteristic for the approach to work.

Table 1. Measured pH Values for NP and QD Dispersions and TBA Solutions at Two Different Concentrations

	0.3 mg/mL	3 mg/mL
ZrP (TBA) in H_2O	7.26	7.73
ZrP (TBA) in acetone	8.04	8.94
nonexfoliated ZrP in H_2O	6.56	6.11
TBA^+OH^- in H_2O	10.82	
TBA^+OH^- in acetone	12.22	
ZnO in methanol	8.10	

To explore the possibility of NPs altering the pH of the dispersion, which could drastically shift the surface charge of the QDs and induce electrostatic stabilization, we measured pH values for various dispersions and solutions at different NP and TBA concentrations (Table 1). The differences between these measurements can be considered negligible, except for the case of TBA in acetone and water. Even so, our control experiments with TBA demonstrate that a large increase in pH does not lead to electrostatic stabilization, and the pH of ZrP modified with TBA in both acetone and water is roughly equivalent to that of ZnO QDs dispersed in methanol.

To begin to assert that NPs can locally alter QD−matrix interactions through a mechanism such as transient polarization of the medium, we must first evaluate the time scales for QD aggregate formation and NP influence on the surrounding medium as a function of ϕ_{ZnO} and ϕ_{ZrP}. For a monodisperse suspension of spherical particles, the average cluster mass is defined by[38]

$$\bar{M} = (R_g^{2D}/r_{ZnO})^{d_f} \tag{3}$$

where R_g^{2D} is the projected radius of gyration of the aggregate and d_f is the fractal dimension. Since we have no reasonable estimate of particle−particle potential, we can begin by making the conservative assumption that QD clusters form by diffusion-limited aggregation, creating fractal structures with $d_f \cong 1.8$.[43,44] The characteristic time, t_a, to form a cluster of average mass is calculated as[38]

$$t_a = t_d[(R_g^{2D}/r_{ZnO})^{d_f} - 1] \tag{4}$$

where t_d is the time for doublet formation expressed by

$$t_d = \frac{\pi\mu_0 r_{ZnO}^3 W}{\phi_{ZnO} kT} \tag{5}$$

with the stability ratio, W, equal to 1 for diffusion-limited aggregation.[38] Note that in these calculations the viscosity was assigned a value of 5000 cP,[42] but the accuracy of this parameter is not critical since viscosity is assumed to impact the diffusive behavior of NPs and QDs with the same linear dependence. Here, we are only interested in relative as opposed to absolute time scales.

The other important time scale is that of NPs sampling their characteristic volume, which is related to $\bar{D}_{ZrP}$ and ϕ_{ZrP}. If one assumes that the ZrP NPs can redisperse QD aggregates within

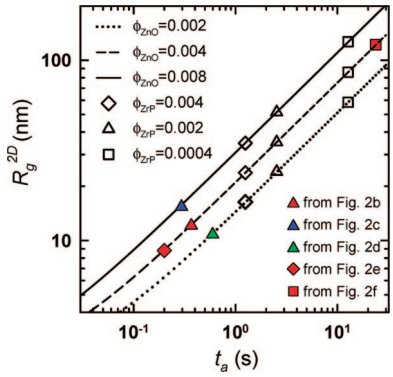

Figure 6. Characteristic time t_a for QD cluster formation of average R_g^{2D} for all ϕ_{ZnO} used in our studies. The open symbols (◇, △, and □) represent calculated times for ZrP NPs to sample their characteristic volume at different values of ϕ_{ZrP}. Filled symbols correspond to R_g^{2D} values estimated from experimental results described in Figure 2B−F.

a surrounding volume defined by r_{ZrP}, then the time scale for a NP to adequately sample its characteristic volume is given by eq 5, where r_{ZrP} is substituted for r_{ZnO} and ϕ_{ZnO} is replaced by an effective NP volume fraction ($\phi_{eff} = 4r_{ZrP}n_{ZrP}/3a$ with a defined as NP thickness and n_{ZrP} the NP number density) that takes into account the difference between doublet formation of spheres and doublet formation of NPs with each NP occupying a swept volume equal to that of a sphere of radius r_{ZrP}. Note that the time scale for rotational diffusion is not included in these analyses for two reasons: an analytical model of platelet diffusion for aspect ratios less than 0.3 is absent from the current literature, and we are not able to predict the minimum separation between a NP and QD cluster at which solvent conditions are changed to a point where QDs return to a disperse state.

The plot in Figure 6 gives the relation between the projected radius of gyration of an average aggregate, R_g^{2D}, and its time for formation for the three experimental values of ϕ_{ZnO} that we examined with HRTEM. Three of the open symbols in Figure 6 correspond to the predicted times for a NP to sample its characteristic volume at a given value of ϕ_{ZrP}. Therefore, the location of these points along each line defines the expected values of R_g^{2D} for given values of ϕ_{ZnO} and ϕ_{ZrP}. If we assume that our epoxy samples serve as a "fossilized" record of the dispersion state within the pre-cross-linked epoxy, the filled symbols in Figure 6 correspond to t_a estimates for average experimental values of R_g^{2D} obtained from HRTEM analyses (see Figure 2B−F and Figure 3A−E). Note that an estimate of R_g^{2D} for aggregates containing fewer than three QDs (see Figure 2D,E and Figure 3C,D) is meaningless, so we have assigned those experimental values a size based on measured cluster diameters from TEM images. The fact that experimental R_g^{2D} values are smaller than that predicted by our rudimentary analyses probably indicate that ZnO QD aggregates form under reaction-limited rather than diffusion-limited conditions, which would change d_f and W in eqs 4 and 5. Nevertheless, these predictions are reasonably close to experimental t_a values, indicating that our assumptions may be fairly realistic. While this result does not validate our hypothesis, it helps to show that our proposed mechanism is a viable explanation of how ZrP NPs are able to disperse ZnO QDs in the solvents and polymeric systems we investigated.

Effectiveness of Nonexfoliated Nanoplatelets. In another control experiment, nonexfoliated (layered, lacking TBA functionalization) ZrP was used in hybrid nanocomposites to determine the importance of incorporating individually dispersed ZrP NPs. To prepare these composites, pristine ZrP was first ultrasonicated in water to achieve a well-dispersed suspension of stacked ZrP platelets. The samples were centrifuged, the supernatant was replaced with acetone, ultrasonication was used again to redisperse and suspend the nonexfoliated NPs, the NPs and ZnO were then incorporated into the epoxy resin, and the samples were cured according to the aforementioned protocol. Figure 7 shows HRTEM images of a hybrid nanocomposite cross section composed of ZnO at $\phi_{ZnO} = 0.004$ and nonexfoliated ZrP NPs at $\phi_{ZrP} = 0.002$. Visible all throughout the cross section are small QD aggregates ~50 nm in diameter and ZrP stacks with QDs bound to their surface through electrostatic interactions, which is explained next.

Inside ZrP layers, hydrogen bonding between surface hydroxyl groups and crystalline water molecules holds the platelets together, and the surface of pristine ZrP is densely occupied by free hydroxyl groups that give rise to a negative surface charge.[29] The same is true for the exterior of the stacked NPs. With regard to colloidal ZnO QDs, it has been shown that, at a pH of ~8, anion vacancies exist on the surface of ZnO QDs, giving rise to a positive surface charge.[45] The pH of our ZnO dispersions in methanol was found to be 8.10; hence, QDs do not associate with exfoliated NPs because adsorbed TBA^+ molecules impart a positive surface charge that repels the positively charged ZnO.[30] On the other hand, in our hybrid nanocomposites containing nonexfoliated ZrP, ZnO is electrostatically attracted to the surface of NPs (Figure 7). Interestingly, the remaining, nonadsorbed ZnO in the epoxy matrix attained a semidispersed state, indicating that ZrP possibly affects the interaction of ZnO with the polymer even when it is not exfoliated into individual

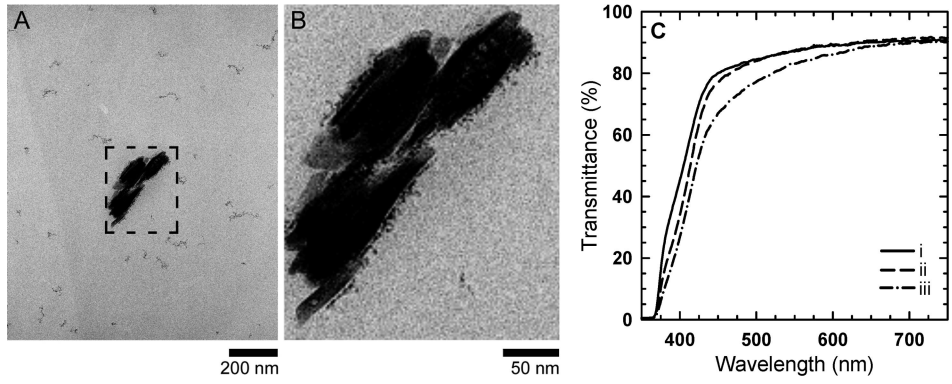

Figure 7. HRTEM images of an epoxy hybrid nanocomposite containing $\phi_{ZnO} = 0.004$ + nonexfoliated ZrP NPs at $\phi_{ZrP} = 0.002$. The overall degree of dispersion is captured in the (A) low-magnification image. In the (B) high-magnification image, the adsorption of QDs onto the ZrP surface is clearly visible. Optical transmittance spectra (C) of (i) neat epoxy (identical to Figure 3A(i)), (ii) epoxy with $\phi_{ZnO} = 0.004$ + exfoliated ZrP NPs at $\phi_{ZrP} = 0.002$ (identical to Figure 3A(iii)), and (iii) $\phi_{ZnO} = 0.004$ + nonexfoliated ZrP NPs at $\phi_{ZrP} = 0.002$ (cross section shown in (A) and (B) of this figure).

platelets. Another and perhaps more intuitive explanation is that the electrostatic adsorption of ZnO onto nonexfoliated ZrP significantly reduces the effective ϕ_{ZnO} within the epoxy matrix, and we are observing a degree of dispersion within a bulk of the matrix equivalent to a composite system with a much lower ZnO concentration. In other words, the nonexfoliated platelets are confining the QDs on their surface and depleting QDs from the remainder of the composite. Interestingly, the optical transmittance spectrum of this composite system is not too different from that of the neat epoxy (Figure 7C). This suggests that there is likely an enhanced degree of dispersion from the addition of ZrP, since scattering from the QD−NP complexes is expected to be evident in the spectrum.

Ongoing Work. To determine if this approach is general with regard to dispersing ZnO QDs in polymers, we have also found that ZrP NPs can tune the dispersion of ZnO in other epoxies and polymer matrices other than epoxy (results not shown here). For example, 5 nm ZnO QDs at $\phi_{ZnO} = 0.016$ have been effectively dispersed within the thermoplastic poly(methyl methacrylate) using ZrP at $\phi_{ZrP} = 0.002$. Additional work is underway to study the effectiveness of using ZrP NPs to disperse different QDs and other oxide nanoparticles, and we hypothesize that ZrP synthesized into other two-dimensional geometries (e.g., rods) and smaller dimensions (e.g., platelets comparable in size to QDs) will require even lower volume fractions to achieve similar QD dispersion states.

Conclusions

The work described here demonstrates a completely new method to disperse ZnO QDs within polymer matrices that does not involve their surface functionalization. Taken together, our findings point to a mechanism by which the presence of ZrP NPs affects QD−matrix and/or QD−QD interactions, perhaps through localized polarization of the medium, in such a way that QDs are continually aggregating and redispersing, the rate of which is related to the concentration of QDs and exfoliated NPs. By simply adjusting the volume fraction of ZrP NPs, the average size of ZnO QD aggregates can be tuned from microns down to individual dots. Our experimental findings suggest that the interaction of ZrP NPs with the polymer, and media such as acetone, changes the thermodynamic character of the matrix, thereby facilitating the dispersion of ZnO QDs through an increase in their favorable interaction with the surrounding medium. Furthermore, dispersion tuning is achieved at low dispersant volume fractions due to the geometry of the nanoplatelets. Future and ongoing work includes dispersion of ZnO QDs in many other polymers using ZrP and other clay NPs with larger dipole moments, dispersion of other nanoparticles with NPs, and investigating the dispersion of ZnO QDs at $\phi_{ZnO} > 0.05$.

Acknowledgment. This research was funded by Kaneka Corporation and the State of Texas (ATP Grant 000512-0311-2003). Dazhi Sun thanks Dr. Zhiping Luo in the Microscopy and Imaging Center (MIC) at TAMU for his assistance with HRTEM imaging and Dr. Jingyi Shen in the Materials Characterization Facility (MCF) at TAMU for her assistance with optical characterization. We also appreciate helpful discussions with Drs. Luyi Sun, Greg Fernandes, and Sam Anekal.

References and Notes

(1) Brus, L. *Appl. Phys. A: Mater. Sci. Process.* **1991**, *53* (6), 465–474.
(2) Alivisatos, A. P. *Science* **1996**, *271* (5251), 933–937.
(3) Michalet, X.; Pinaud, F. F.; Bentolila, L. A.; Tsay, J. M.; Doose, S.; Li, J. J.; Sundaresan, G.; Wu, A. M.; Gambhir, S. S.; Weiss, S. *Science* **2005**, *307* (5709), 538–544.
(4) Alivisatos, A. P. *J. Phys. Chem.* **1996**, *100* (31), 13226–13239.
(5) Murray, C. B.; Norris, D. J.; Bawendi, M. G. *J. Am. Chem. Soc.* **1993**, *115* (19), 8706–8715.
(6) Koch, U.; Fojtik, A.; Weller, H.; Henglein, A. *Chem. Phys. Lett.* **1985**, *122* (5), 507–510.
(7) Spanhel, L.; Anderson, M. A. *J. Am. Chem. Soc.* **1991**, *113* (8), 2826–2833.
(8) Kagan, C. R.; Murray, C. B.; Bawendi, M. G. *Phys. Rev. B* **1996**, *54* (12), 8633–8643.
(9) Kagan, C. R.; Murray, C. B.; Nirmal, M.; Bawendi, M. G. *Phys. Rev. Lett.* **1996**, *76* (9), 1517–1520.
(10) Artemyev, M. V.; Bibik, A. I.; Gurinovich, L. I.; Gaponenko, S. V.; Woggon, U. *Phys. Rev. B* **1999**, *60* (3), 1504–1506.
(11) Yang, R. D.; Tripathy, S.; Li, Y. T.; Sue, H. J. *Chem. Phys. Lett.* **2005**, *411* (1−3), 150–154.
(12) Xiong, H. M.; Zhao, X.; Chen, J. S. *J. Phys. Chem. B* **2001**, *105* (42), 10169–10174.
(13) Huynh, W. U.; Dittmer, J. J.; Alivisatos, A. P. *Science* **2002**, *295* (5564), 2425–2427.
(14) Beek, W. J. E.; Wienk, M. M.; Janssen, R. A. J. *Adv. Mater.* **2004**, *16* (12), 1009++.
(15) Sun, D.; Miyatake, N.; Sue, H. J. *Nanotechnology* **2007**, *18* (21), --.
(16) Khrenov, V.; Klapper, M.; Koch, M.; Mullen, K. *Macromol. Chem. Phys.* **2005**, *206* (1), 95–101.
(17) Li, Y. Q.; Fu, S. Y.; Mai, Y. W. *Polymer* **2006**, *47* (6), 2127–2132.
(18) Guo, L.; Yang, S. H.; Yang, C. L.; Yu, P.; Wang, J. N.; Ge, W. K.; Wong, G. K. L. *Chem. Mater.* **2000**, *12* (8), 2268–2274.
(19) Kim, S. W.; Kim, S.; Tracy, J. B.; Jasanoff, A.; Bawendi, M. G. *J. Am. Chem. Soc.* **2005**, *127* (13), 4556–4557.
(20) Peng, X. G.; Wickham, J.; Alivisatos, A. P. *J. Am. Chem. Soc.* **1998**, *120* (21), 5343–5344.
(21) Kickelbick, G. *Prog. Polym. Sci.* **2003**, *28* (1), 83–114.
(22) Hooper, J. B.; Schweizer, K. S. *Macromolecules* **2006**, *39* (15), 5133–5142.
(23) Sun, D. Z.; Wong, M. H.; Sun, L. Y.; Li, Y. T.; Miyatake, N.; Sue, H. J. *J. Sol-Gel Sci. Technol.* **2007**, *43* (2), 237–243.
(24) Sun, L. Y.; Boo, W. J.; Sue, H. J.; Clearfield, A. *New J. Chem.* **2007**, *31* (1), 39–43.
(25) Sun, L. Y.; Boo, W. J.; Sun, D. H.; Clearfield, A.; Sue, H. J. *Chem. Mater.* **2007**, *19* (7), 1749–1754.
(26) Kojima, Y.; Usuki, A.; Kawasumi, M.; Okada, A.; Fukushima, Y.; Kurauchi, T.; Kamigaito, O. *J. Mater. Res.* **1993**, *8* (5), 1185–1189.
(27) Alexandre, M.; Dubois, P. *Mater. Sci. Eng., R* **2000**, *28* (1−2), 1–63.
(28) Giannelis, E. P. *Adv. Mater.* **1996**, *8* (1), 29000.
(29) Clearfield, A. *Annu. Rev. Mater. Sci.* **1984**, *14*, 205–229.
(30) Kim, H. N.; Keller, S. W.; Mallouk, T. E.; Schmitt, J.; Decher, G. *Chem. Mater.* **1997**, *9* (6), 1414–1421.
(31) Koylu, U. O.; Faeth, G. M.; Farias, T. L.; Carvalho, M. G. *Combust. Flame* **1995**, *100* (4), 621–633.
(32) Brasil, A. M.; Farias, T. L.; Carvalho, M. G. *J. Aerosol Sci.* **1999**, *30* (10), 1379–1389.
(33) Iba, H.; Chang, T.; Kagawa, Y. *Compos. Sci. Technol.* **2002**, *62* (15), 2043–2052.
(34) Chailleux, E.; Salvia, M.; Jaffrezic-Renault, N.; Matejec, V.; Kasik, I. *Smart Mater. Struct.* **2001**, *10* (2), 194–202.
(35) Batchelor, G. K. *J. Fluid Mech.* **1976**, *74*, 1–29.
(36) Shimizu, H. *J. Chem. Phys.* **1962**, *37* (4), 765000.
(37) Brenner, H.; Condiff, D. W. *J. Colloid Interface Sci.* **1974**, *47* (1), 199–264.
(38) Russel, W. B.; Saville, D. A.; Schowalter, W. R. *Colloidal Dispersions*; Cambridge University Press: New York, 1989.
(39) Tuteja, A.; Mackay, M. E.; Narayanan, S.; Asokan, S.; Wong, M. S. *Nano Lett.* **2007**, *7*, 1276–1281.
(40) van der Kooij, F. M.; Philipse, A. P.; Dhont, J. K. G. *Langmuir* **2000**, *16* (12), 5317–5323.
(41) Liu, J.; Cao, D. P.; Zhang, L. Q. *J. Phys. Chem. C* **2008**, *112* (17), 6653–6661.
(42) Ellis, B. *Chemistry and Technology of Epoxy Resins*, 1st ed.; Blackie Academic & Professional: London, 1993; p xixi.
(43) Meakin, P. *Phys. Rev. Lett.* **1983**, *51* (13), 1119–1122.
(44) Kolb, M.; Botet, R.; Jullien, R. *Phys. Rev. Lett.* **1983**, *51* (13), 1123–1126.
(45) Kamat, P. V.; Patrick, B. *J. Phys. Chem.* **1992**, *96* (16), 6829–6834.

MA801979C